ChemPubSoc Europe

DOI: 10.1002/open.201500106

Open Access ChemistryOPEN Full Papers

Influence of Ag^+ on the Magnetic Response of [2.2.2]Paracyclophane: NMR Properties of a Prototypical Organic Host for Cation Binding Based on DFT Calculations

Desmond MacLeod Carey,[a] Tatiana Gomez,[a] Cesar Morales-Verdejo,[b] and Alvaro Muñoz-Castro*[a]

The complexation of metal cations into a host–guest situation is particularly well exemplified by [2.2.2]paracyclophane and Ag^I, which leads to a strong cation–π interaction with a specific face of the host molecule. Through this study we sought a deeper understanding of the effects the metal center has on the NMR spectroscopic properties of the prototypical organic host, generating theoretical reasons for the observed experimental results with an aim to determine the role of the cation–π interaction in a host–guest scenario. From an analysis of certain components of the induced magnetic field and the ^{13}C NMR shielding tensor under its own principal axis system (PAS), the local and overall magnetic behavior can be clearly described. Interestingly, the magnetic response of such a complex exhibits a large axis-dependent behavior, which leads to an overall shielding effect for the coordinating carbon atoms and a deshielding effect for the respective uncoordinated counterparts, evidence that complements previous experimental results. This proposed approach can be useful to gain further insight into the local and overall variation of NMR shifts for host–guest pairs involving both inorganic and organic hosts.

Introduction

The formation of cation–π systems is a process that plays a central role in many chemical and biological systems.[1–3] Cation–π interactions continue to attract attention owing to their potential importance in the areas of molecular recognition, metal-ion sensing, electrical conductors, and photoresponsive devices.[1–6] It is known that π-prismands and certain hydrocarbon cyclophanes are capable of forming π-complexes with small metal cations, in which arene rings act as the main π-electron donors in the resulting complex.[7] Such structures have also been studied as novel subjects in the formation of conjugated polymers for use in materials with interesting optical and electrochemical properties.[8]

[2.2.2]Paracyclophane ([2.2.2]pCp) and related structures[5,9–14] have been recognized as effective π-prismands for cation–π interactions since Pierre et al.[15] reported the early preparation of a silver–trifluoromethanesulfonate complex as the first member of such a compound class, resulting in a host–guest situation. [2.2.2]pCp exhibits three aromatic rings which are held at short distances in a *para* disposition connected by $-(CH_2)_2-$ bridges,[8] allowing π–π interactions between their inner faces.[16,17] This geometry leads to a polyaromatic receptor cavity suitable for several metal cations[5,8–14] involving the aromatic rings. In the original report[15] the conformation of the complex [2.2.2]pCp–Ag^I was speculated to have the Ag^I cation at the center of the organic cavity. Further structural studies[18] revealed that in such a π-prismand complex, the silver cation is bonded to one face of the cavity involving a C=C double bond for each arene moiety, resulting in a $\eta^2:\eta^2:\eta^2$ coordination mode (or an overall η^6) because of symmetry and energetic considerations, as was recently described.[19]

In general, solution- and solid-phase experimental studies of cation–π interactions frequently use NMR spectroscopic experiments.[8,20,21] Among other nondestructive characterization methods, NMR spectroscopy is a valuable tool for assessing any variations in the chemical environment of an organic host that might occur upon complex formation with a metal center. The magnetic response at the nuclei, which account for usual NMR experiments,[22] can be conveniently generalized through space, leading to a graphical representation of the short- and

[a] Dr. D. MacLeod Carey, Dr. T. Gomez, Dr. A. Muñoz-Castro
Facultad de Ingeniería, Universidad Autonoma de Chile
Llano Subercaceaux 2801, San Miguel, Santiago 780-0026 (Chile)
E-mail: alvaro.munoz@uautonoma.cl

[b] Dr. C. Morales-Verdejo
Departamento de Ciencias Químicas y Biológicas
Universidad Bernardo O'Higgins, General Gana 1780, Santiago 8370993 (Chile)

Supporting information for this article is available on the WWW under http://dx.doi.org/10.1002/open.201500106.

long-range magnetic behavior driven by the presence of induced currents[23–27] from certain atoms or functional groups. This allows a deeper understanding of the through-space or through-bond mechanism from which neighboring groups influence the chemical shift and other NMR parameters of a given probe nucleus.

As part of our ongoing research on magnetic properties,[28–30] we set out to study the influence of Ag^{I} on the magnetic response of the organic host, namely [2.2.2]pCp, upon formation of the representative cation–π host–guest complex, by using density functional theory (DFT). In addition to the local magnetic properties at certain nuclei, we also describe the molecular response under a uniform external magnetic field (B^{ext}) by mapping the induced magnetic field (B^{ind}) quantity, which reflects long- and short-range magnetic responses. Such terms are related to the second-rank shielding tensor (σ_{ij}) expressed in ppm units of B^{ext} (ppm), according to $B^{ind}_j = \sigma_{ij} B^{ext}_i$.[22–27] Here, the *i* and *j* sub-indexes are conveniently related to the *x*, *y*, and *z* axes of a molecule-fixed Cartesian coordinate system for the through-space representation, in contrast to the principal axis system (PAS) representation of a tensor centered in a nucleus where $i,j = 1,2,3$.

Computational Details

DFT calculations were performed by using the ADF 2012 code,[31] incorporating both scalar and spin-orbit corrections via the two-component ZORA Hamiltonian.[32] The quadruple-ζ Slater basis set plus four polarization functions (QZ4P) were used within the generalized gradient approximation (GGA) according to the Becke–Perdew (BP86) exchange-correlation functional[33] by using the optimized structure taken from ref. [19]. The molecular response (B^{ind}) to an external field (B^{ext}) through space is given by the shielding tensor ($\sigma_{(r)}$),[22] which relates the induced and applied magnetic field in B^{ext}. Representation of $\sigma_{(r)}$ as a function of Cartesian coordinates describes the shielding toward B^{ext} in molecular space, reflecting long- and short-range magnetic responses that arise by induced electronic currents under an external field.[22] The Cartesian $\sigma_{(r)}$ quantities were calculated within the NMR module of the ADF 2012 code, which uses the gauge-including atomic orbitals (GIAO) formalism to circumvent the gauge-origin problem of a finite basis set, in a two-dimensional grid of 10×10 Å^2 with a separation of 0.318 Å. The graphical representation of the shielding tensor was obtained based on the method reported by Autschbach and co-workers,[34] considering a function written in spherical coordinates representing the $f(r) = \Sigma_{ij} r_i r_j \sigma_{ij}$ expression centered at the respective nucleus, depicting its orientation and magnitude.

Results and Discussion

[2.2.2]Paracyclophane can display several conformations given by the relative orientation of the $-(CH_2)_2-$ bridges[35] ranging from a D_3 to a C_2 structure. The early characterization of $[Ag([2.2.2]pCp)]^+$ by NMR solution experiments was later corroborated structurally, denoting a coordination of the Ag^+ center above the center of the π-prismane ligand.[15,18] Such a coordination mode can be ascribed to a $\eta^2{:}\eta^2{:}\eta^2$ hapticity, in which two aromatic carbon atoms of each six-membered ring are involved in the interaction.[19] The characterized structure of $[Ag([2.2.2]pCp)]^+$ depicts slight variations from the C_3 point group (RMSD: 0.134 Å), which can be attributed to crystal packing and counter-ion effects. Such a structure results from [2.2.2]pCp in a D_3 conformation, in which the inclusion of Ag^+ breaks the perpendicular C_2 rotation axis, leading to the consequent symmetry depicting three equivalent aromatic rings (Figure 1).

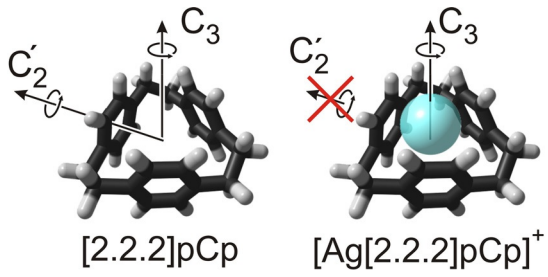

Figure 1. Optimized structures of [2.2.2]paracyclophane and [2.2.2]paracyclophane–Ag^{I}, depicting the decrease in symmetry upon inclusion of Ag^{I} from a D_3 {C_3;$3C_2'$} to a C_3 {C_3} point group.

The optimized structure[19] is consistent with the experimental C_3 structure[18] (RMSD: 0.011 Å from a C_3 point group), where the silver center is located 1.383 Å above the center (exp.: 1.433 Å), in good agreement with the experimental data.[18] The averaged Ag–C distance of 2.599 Å (exp.: 2.588 Å) is longer than that observed for the simplest model of a cation–olefin complex, namely $[Ag(\eta^2\text{-}C_2H_4)_3]^+$, due to strain within the π-prismane structure. The conformational changes adopted to maximize the cation–π interaction are calculated to destabilize the organic structure by 3.93 kcal mol^{-1}.[19] The interaction energy of [2.2.2]pCp and Ag^+ has been estimated to be −100.1 kcal mol^{-1}, slightly favorable relative to the prototypical noncovalent cation–π complex $[Ag(\eta^2\text{-}C_2H_4)_3]^+$ (−92.79 kcal mol^{-1} at the same level of theory), which is indicative of a lesser ligand to metal charge transfer in the latter, in agreement with the natural population analysis denoting a charge distribution of $[Ag^{0.67+}[2.2.2]pCp^{0.33+}]$[19] and $[Ag^{0.85+}(C_2H_4)_3^{0.15+}]$. Thus, [2.2.2]pCp ensures a stronger formation for the host–guest situation, as has been proven for Ag^+[15] taking several polyaromatic structures into account.

Because of the C_3 symmetry point group of $[Ag([2.2.2]pCp)]^+$, six chemically different aromatic carbon types are advised from theoretical ^{13}C NMR calculations, as depicted in Figure S1 and Table S1 (Supporting Information), given by C(1) = 137.9, C(4) = 137.8, C(2) = 119.7, C(3) = 118.6, C(5) = 133.5, and C(6) = 130.0 ppm, obtained as $\delta_{ij} = \sigma^{TMS} - \sigma_{ij}$[22] ($\sigma^{TMS} = 193.10$ ppm). To take into account the dynamic scenario resulting from the solution-state NMR experiment,[15] the related nuclei were averaged into three main chemically different groups of aromatic carbon atoms, namely **C1**, **C2**, and **C3** (Figure 2). Such groups are composed of C(1)–C(4), C(2)–C(3), and C(5)–C(6), depicting

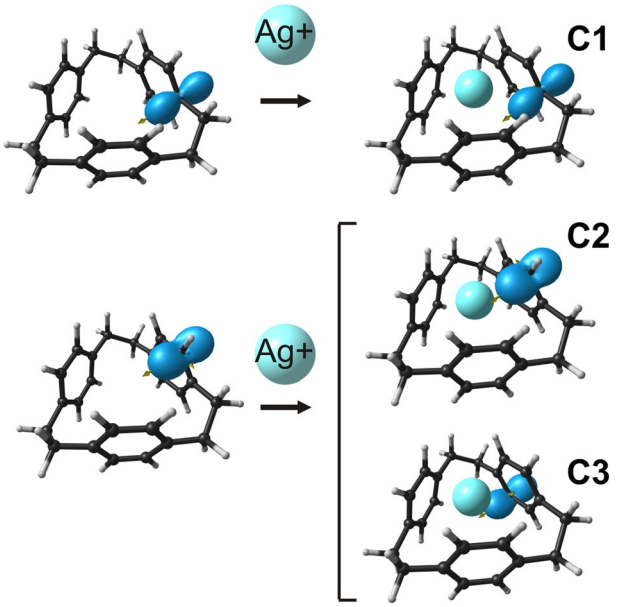

Figure 2. Orientation and magnitude of the absolute shielding (σ_{ij}) for **C1**, **C2**, and **C3** before and after the inclusion of Ag^{I}.

para-, upper-*meta*, and lower-*meta* carbons, respectively (Figure 2). Hence, the ^{13}C NMR shifts amount to 137.8 ppm for **C1**, 119.1 ppm for **C2**, and 131.8 ppm for **C3** (Table 1).

For isolated [2.2.2]pCp the experimentally characterized ^{13}C NMR signals for the aromatic ring are located at 136.56 and 128.35 ppm, corresponding respectively to the *para*- and *meta*-carbon atoms.[15] Upon formation of the cation–π system, the *para*-carbon is shifted slightly downfield to 138.19 ppm, whereas the four *meta*-carbons are shifted highfield (125.95 ppm). However, as the coordination mode of Ag^+ involves the upper face of [2.2.2]pCp breaking the perpendicular C_2' symmetry axis (Figure 1), two chemically different groups of *meta*-carbons should be observed, suggesting that the carbons in the above and below faces (i.e., **C2** and **C3**) are averaged to one peak located at ^{13}C NMR 125.95 ppm.[15]

Table 1. Isotropic and principal components of the absolute shielding, and the corresponding chemical shift denoting the respective experimental data. All values are in ppm.

pCp	σ_{11}	σ_{22}	σ_{33}	σ_{iso}	δ_{iso}		δ_{exp}[b]
C1	−33.77	27.37	178.15	57.25	135.85		136.56
C2	−34.09	60.73	170.40	65.68	127.42		128.35
C3	−34.08	60.72	170.38	65.67	127.43		
Ag^+pCp							
C1	−35.38	20.76	180.40	55.26	137.84		138.19
C2	−22.06	68.26	175.68	73.96	119.14	125.46[a]	125.95
C3	−39.31	50.44	172.82	61.32	131.78		
	$\Delta\sigma_{11}$	$\Delta\sigma_{22}$	$\Delta\sigma_{33}$	$\Delta\sigma_{iso}$	$\Delta\delta$		
ΔC1	−1.61	−6.61	2.25	−1.99	1.99		
ΔC2	12.03	7.53	5.28	8.28	−8.28		
ΔC3	−5.23	−10.29	2.45	−4.36	4.36		

[a] Average between δ_{iso} from **C2** and **C3**, accounting for the experimentally assigned peak. [b] Data from ref. [15].

Consequently, the theoretical ^{13}C NMR chemical shifts (Table 1) denote two different groups for such a position, where the carbons located at the upper face, where the Ag^+ ion is located, are shifted upfield to 119.14 ppm. In contrast, the group of *meta*-carbons located in the opposite face exhibit a downfield shift toward 131.78 ppm, revealing two different chemical environments for the above and below π-faces. Interestingly, the average between the theoretically assigned signals for both groups of *meta*-carbons reproduces the characterized signal for such carbons well (Table 1), denoting an averaged value of 125.46 ppm; this suggests a signal coalescence for the two different groups of *meta*-carbons in the experimental report. Thus, the calculated values agree well with the experimental data, suggesting three different signals instead of two for the aromatic carbons at δ_{iso} of 137.8 (**C1**), 119.1 (**C2**), and 131.8 (**C3**) ppm, respectively. The calculated variation in the ^{13}C NMR shift for ethyl carbon atoms exhibits a similar slight upfield trend ($\Delta\delta = 0.76$ ppm), similar to that observed experimentally ($\Delta\delta = 0.55$ ppm).

To exploit the information given from such tensor (σ_{ij}, $i,j = 1,2,3$), we provide a graphical representation that describes the three principal components (eigenvalues) of the diagonalized tensor in its own principal axis system (PAS)[15,36] (Figure 2). Here, σ_{ij} is oriented in the molecular frame which describes the orientation, magnitude, and sign of such a response, relevant parameters that are reduced to a single value when the isotropic chemical shift is usually employed.[36] The principal components of the shielding tensor at the nuclei are designated by σ_{11}, σ_{22}, and σ_{33}, according to $\sigma_{11} \leq \sigma_{22} \leq \sigma_{33}$, reserving the *x*, *y*, and *z* suffixes for the through-space representation of the magnetic response (see below). For **C1**, **C2**, and **C3**, the most shielded component, namely σ_{33}, points toward the center of the structure (Figure 2), whereas σ_{11} and σ_{22} are located within the C_6 plane; σ_{11} is located through the C–H bond, and the latter (σ_{22}) is oriented toward the carbon neighbors. The familiar upfield/downfield terms used in NMR interpretations remain, which are directly related to the variation of σ in theoretical calculations.[22]

For **C1**, σ_{33} is shifted by ~2.25 ppm toward the upfield region, whereas σ_{11} and σ_{22} are shifted downfield. In such a nucleus, the main difference leading to the chemical shift variations is taken into account by the σ_{22} component (Table 1). The shift of the σ_{33} PAS component located at **C2** amounts to 5.28 ppm upfield; however, despite the orientation of such a component toward the Ag^+ center, it is not the more influenced term of the respective shielding tensor. For **C2**, the σ_{11} component, which is oriented through the C–H bond, is largely upfield shifted by ~12.03 ppm, followed by the σ_{22} component by ~7.53 ppm. In contrast, **C3** exhibits a lesser σ_{33} shift, denoting a larger downfield shift for σ_{22} of about −10.29 ppm, and of −5.23 ppm for σ_{11}. From Figure 3, the differences between each principal component before and after the inclusion of the Ag^+ center are described, where it can be clearly seen that the σ_{11} and σ_{22} components are the more influ-

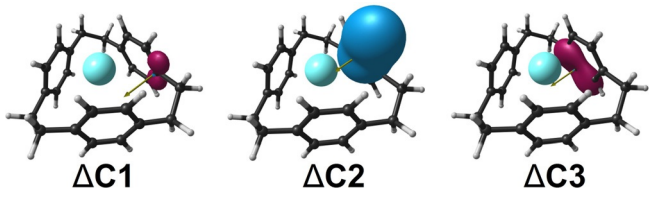

Figure 3. Magnitude in variation of the principal components for **C1**, **C2**, and **C3** (isovalue ±5 ppm), denoting shielding for positive values in blue, and deshielding for negative values in red.

enced terms in the nuclear shielding of the representative carbon atoms. As result, the atoms in the aromatic ring located in the face below are deshielded, whereas those in the upper face are shielded, and hence the through-space effect due to inclusion of the Ag^+ ion is of a shielding nature.

The local magnetic response at each nucleus can be generalized to any point in space, which can be carried out on the basis of the NICS procedure reported by von Ragué Schleyer et al.,[37,38] leading to a map representation of the induced magnetic field (in B^{ext}) over space. The molecular response to a uniform external magnetic field (B^{ext}) leads to an induced electronic current density, which in turn yields a non-uniform induced magnetic field ($B_{(r)}^{ind}$)[39,40] related by the magnetic shielding tensor $\sigma_{(r)}$ according to:

$$B_i^{ind} = -\sigma_{ij} B_i^{ext} \quad (1)$$

for which the *i* and *j* suffixes are related to the molecule-fixed Cartesian axis (*i,j* = *x,y,z*).

The through-space isotropic component that accounts for the overall magnetic behavior of $[Ag([2.2.2]pCp)]^+$ ($\sigma_{iso} = 1/3(\sigma_{xx}+\sigma_{yy}+\sigma_{zz})$) is given in Figure 3. When NMR experiments are conducted in solution, rapid tumbling of the solute molecules leads to an averaging of molecular orientations. In many cases, this leads to sharp peaks, and isotropic chemical shift data may be obtained as the motion of the solute molecules is isotropic over the time scale of the NMR experiment. Such an isotropic component, also termed NICS, exhibits an averaged magnetic behavior that accounts for the rapid molecular tumbling, related to solution-phase NMR experiments. The map representation of σ_{iso} reveals the additive interaction of the shielding regions ($\sigma > 0$) between the paracyclophane structure and the metal cation. Thus, the through-space shielding effect of the Ag^+ center, which influences the local σ_{33} principal component of the representative **C1**, **C2**, and **C3** carbon atoms, is spatially characterized to be, to a large extent, in the face above the center, and, to a lesser degree, in the opposite face, in agreement with the discussion above supporting the differences between the two groups of *meta*-carbons.

Due to the symmetry of the structure, the magnetic response of $[Ag([2.2.2]pCp)]^+$ exhibits an axis-dependent behavior, which can be accounted for by the analysis of certain components of σ_{ij}. The analysis of σ_{zz}, σ_{xx}, and σ_{yy} (Figure 3) denotes the difference when the external field is applied from the *z*, *x*, and *y* axes, respectively. From σ_{zz}, the enhancement of the shielding region near the Ag^+ center is located along the

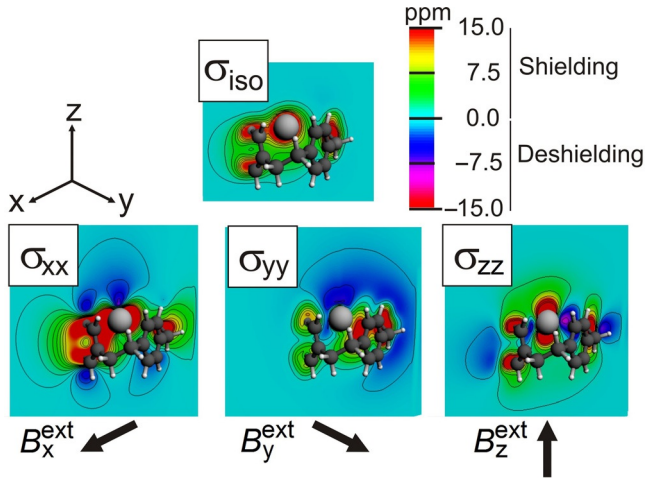

Figure 4. Map representation of through-space magnetic response (induced magnetic field), depicting the isotropic component and certain components of such tensor depicting the response under a specific orientation of the applied field.

z axis with a complementary deshielding region perpendicular to such axis. Thus, considering this particular example, the silver center will deshield the closer carbon atoms of [2.2.2]pCp (Figure 4).

When the external field is contained in the *x* axis, the aromatic ring experiences an induced ring current because it is located perpendicular to such a field as a result of the ring current effect.[41–43] Interestingly, the Ag^+ center again exhibits a shielding region contained in the axis of the applied field, with the respective perpendicular deshielding region. From the σ_{xx} component the overlap of the shielding regions from the aromatic ring and the metal center is observed. The deshielding region originating from the metal center decreased by a large extent at the inner region of the paracyclophane structure, and remains as a deshielding zone at the outer region.

Interestingly, when the field is applied from the *y* axis, a large perpendicular deshielding region is observed outside the [2.2.2]pCp structure, which results from the additive interaction between both metallic and ligand deshielding regions. In contrast, inside the π-prismane a shielding response remains, resulting from the destructive deshielding–shielding interaction.

Conclusions

In summary, variation in the magnetic behavior of the [2.2.2]paracyclophane host upon formation of a prototypical strong cation–π complex involving Ag^I has been studied in order to exploit the information given by solution-state NMR experiments. From the analysis of certain components of induced magnetic field and ^{13}C NMR shielding tensor under its own principal axis system (PAS), the local and overall magnetic behavior is described, denoting a large axis-dependent behavior which leads to a shielding effect for the coordinating carbons, and a deshielded effect for the respective uncoordinated counterpart, evidence that complements the earlier experi-

mental data. The approach described herein can be useful for gaining deeper insight into the local and overall variations in experimentally characterized NMR shifts for host–guest pairs involving both inorganic and organic hosts.

Acknowledgements

The authors are thankful for financial support from FONDECYT grants 1140359 and 1131123.

Keywords: cation–π interactions · host–guest systems · NMR spectroscopy · shielding · silver

[1] J. W. Steed, J. L. Atwood, *Supramolecular Chemistry*, Wiley-VCH, Weinheim, Germany, **2000**.
[2] J. P. Gallivan, D. A. Dougherty, *Proc. Natl. Acad. Sci. USA* **1999**, *96*, 9459–9464.
[3] J. C. Ma, D. A. Dougherty, *Chem. Rev.* **1997**, *97*, 1303–1324.
[4] K. S. Kim, P. Tarakeshwar, J. Y. Lee, *Chem. Rev.* **2000**, *100*, 4145–4186.
[5] V. J. Chebny, M. Banerjee, R. Rathore, *Chem. Eur. J.* **2007**, *13*, 6508–6513.
[6] A. S. Mahadevi, G. N. Sastry, *Chem. Rev.* **2013**, *113*, 2100–2138.
[7] a) F. Vögtle, *Cyclophane Chemistry*, Wiley, Chichester, **1993**; b) R. Gleiter, H. Hopf, *Modern Cyclophane Chemistry*, Wiley-VCH, Weinheim, Germany, **2004**.
[8] a) F. Salhi, D. M. Collard, *Adv. Mater.* **2003**, *15*, 81–85; b) Y. Morisaki, S. Ueno, A. Saeki, A. Asano, S. Seki, Y. Chujo, *Chem. Eur. J.* **2012**, *18*, 4216–4224; c) M. Montanari, A. Bugana, A. K. Sharma, D. Pasini, *Org. Biomol. Chem.* **2011**, *9*, 5018–5020.
[9] G. Pierre, P. Baret, P. Chautemps, J.-L. Pierre, *Electrochim. Acta* **1983**, *28*, 1269–1287.
[10] H. C. Kang, A. W. Hanson, B. Eaton, V. Boelelheide, *J. Am. Chem. Soc.* **1985**, *107*, 1979–1985.
[11] H. Schmidbaur, R. Hager, B. Huber, G. Müller, *Angew. Chem. Int. Ed. Engl.* **1987**, *26*, 338–340; *Angew. Chem.* **1987**, *99*, 354–356.
[12] T. Probst, O. Steigelmann, J. Riede, H. Schmidbaur, *Angew. Chem. Int. Ed. Engl.* **1990**, *29*, 1397–1398; *Angew. Chem.* **1990**, *102*, 1471–1473.
[13] P. Debroy, S. V. Lindeman, R. Rathore, *J. Org. Chem.* **2009**, *74*, 2080–2087.
[14] J. Gross, G. Harder, A. Siepen, J. Harren, F. Vögtle, H. Stephan, K. Gloe, B. Ahlers, K. Cammann, K. Rissanen, *Chem. Eur. J.* **1996**, *2*, 1585–1595.
[15] J. L. Pierre, P. Baret, P. Chautemps, M. Armand, *J. Am. Chem. Soc.* **1981**, *103*, 2986–2988.
[16] P. J. Dyson, D. G. Humphrey, J. E. McGrady, P. Suman, D. Tocher, *J. Chem. Soc. Dalton Trans.* **1997**, 1601–1606.
[17] F. Imashiro, Z. Yoshida, I. Tabushi, *Tetrahedron* **1973**, *29*, 3521–3526.
[18] C. Cohen-Addad, P. Baret, P. Chautemps, J.-L. Pierre, *Acta Crystallogr. Sect. C* **1983**, *39*, 1346–1349.
[19] C. Olea Ulloa, M. Ponce-Vargas, R. M. Piccoli, G. F. Caramori, G. Frenking, A. Muñoz-Castro, *RSC Adv.* **2015**, *5*, 7803–7811.
[20] D. L. Bryce, S. Adiga, E. K. Elliott, G. W. Gokel, *J. Phys. Chem. A* **2006**, *110*, 13568–13577.
[21] G. Wu, V. Terskikh, *J. Phys. Chem. A* **2008**, *112*, 10359–10364.
[22] M. Kaupp, M. Bühl, V. G. Malkin, *Calculation of NMR and EPR parameters. Theory and Applications*, Wiley-VCH, Weinheim, **2004**.
[23] S. Klod, E. Kleinpeter, *J. Chem. Soc. Perkin Trans. 2* **2001**, 1893–1898.
[24] T. Heine, C. Corminboeuf, G. Seifert, *Chem. Rev.* **2005**, *105*, 3889–3910.
[25] G. Merino, T. Heine, G. Seifert, *Chem. Eur. J.* **2004**, *10*, 4367–4371.
[26] M. Baranac-Stojanović, *RSC Adv.* **2014**, *4*, 308–321.
[27] N. D. Charistos, A. G. Papadopoulos, M. P. Sigalas, *J. Phys. Chem. A* **2014**, *118*, 1113–1122.
[28] M. Ponce-Vargas, A. Muñoz-Castro, *Phys. Chem. Chem. Phys.* **2014**, *16*, 13103–13111.
[29] A. Muñoz-Castro, *J. Phys. Chem. C* **2012**, *116*, 17197–17203.
[30] A. Muñoz-Castro, *Chem. Phys. Lett.* **2011**, *517*, 113–115.
[31] Amsterdam Density Functional (ADF) Code, Vrije Universiteit, Amsterdam (The Netherlands).
[32] E. van Lenthe, E. J. Baerends, J. G. Snijders, *J. Chem. Phys.* **1994**, *101*, 9783–9792.
[33] a) A. D. Becke, *Phys. Rev. A* **1988**, *38*, 3098–3100; b) J. P. Perdew, *Phys. Rev. B* **1986**, *33*, 8822–8824.
[34] E. Zurek, C. J. Pickard, J. Autschbach, *J. Phys. Chem. C* **2008**, *112*, 11744–11750.
[35] a) E. G. Buchanan, J. C. Dean, T. S. Zwier, E. L. Sibert III, *J. Chem. Phys.* **2013**, *138*, 064308; b) E. G. Buchanan, T. S. Zwier, *J. Phys. Chem. A* **2014**, *118*, 8583–8596.
[36] a) R. S. Drago, *Physical Methods in Chemistry*, W. B. Saunders, Philadelphia, **1977**, ch. VII; b) M. J. Duer, *Introduction to Solid-State NMR Spectroscopy*, Blackwell Publishing, Oxford, **2004**.
[37] P. von Ragué Schleyer, C. Maerker, A. Dransfeld, H. Jiao, H. J. R. Hommes, *J. Am. Chem. Soc.* **1996**, *118*, 6317–6318.
[38] Z. Chen, C. S. Wannere, C. Corminboeuf, R. Puchta, P. von Ragué Schleyer, *Chem. Rev.* **2005**, *105*, 3842–3888; Schleyer, *Chem. Rev.* **2005**, *105*, 3842–3888.
[39] R. Islas, T. Heine, G. Merino, *Acc. Chem. Res.* **2012**, *45*, 215–228.
[40] R. Carion, V. Liégeos, B. Champagne, D. Bonifazi, S. Pelloni, P. Lazzeretti, *J. Phys. Chem. Lett.* **2010**, *1*, 1563–1568.
[41] P. von Ragué Schleyer, H. Jiao, *Pure Appl. Chem.* **1996**, *68*, 209–218.
[42] U. Fleischer, W. Kutzelnigg, P. Lazzeretti, V. Mühlenkamp, *J. Am. Chem. Soc.* **1994**, *116*, 5298–5306.
[43] W. H. Flygare, R. C. Benson, *J. Am. Chem. Soc.* **1970**, *92*, 7523–7529.

Received: April 19, 2015
Published online on June 26, 2015

